

## Ultrafast terahertz transmission ellipsometry of $\text{YMn}_2\text{O}_5$ electromagnons

Hyosub Kim, Minwoo Yi, Xueyun Wang, Sang-Wook Cheong, and Jaewook Ahn

Citation: *Appl. Phys. Lett.* **101**, 242911 (2012); doi: 10.1063/1.4772206

View online: <http://dx.doi.org/10.1063/1.4772206>

View Table of Contents: <http://apl.aip.org/resource/1/APPLAB/v101/i24>

Published by the [American Institute of Physics](#).

### Related Articles

Nanosecond pulsed laser blackening of copper  
*Appl. Phys. Lett.* **101**, 231902 (2012)

Ultrafast time dynamics studies of periodic lattices with free electron laser radiation  
*J. Appl. Phys.* **112**, 093519 (2012)

Pulsed terahertz radiation due to coherent phonon-polariton excitation in 110 ZnTe crystal  
*J. Appl. Phys.* **112**, 093110 (2012)

Terahertz emission from cubic semiconductor induced by a transient anisotropic photocurrent  
*J. Appl. Phys.* **112**, 073115 (2012)

Antenna effect in laser assisted atom probe tomography: How the field emitter aspect ratio can enhance atomic scale imaging  
*Appl. Phys. Lett.* **101**, 153101 (2012)

### Additional information on *Appl. Phys. Lett.*

Journal Homepage: <http://apl.aip.org/>

Journal Information: [http://apl.aip.org/about/about\\_the\\_journal](http://apl.aip.org/about/about_the_journal)

Top downloads: [http://apl.aip.org/features/most\\_downloaded](http://apl.aip.org/features/most_downloaded)

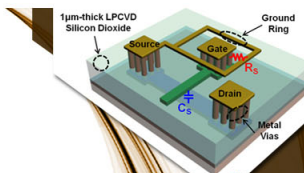
Information for Authors: <http://apl.aip.org/authors>

## ADVERTISEMENT



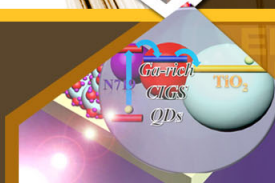
**EXPLORE WHAT'S  
NEW IN APL**

**SUBMIT YOUR PAPER NOW!**



### **SURFACES AND INTERFACES**

Focusing on physical, chemical, biological, structural, optical, magnetic and electrical properties of surfaces and interfaces, and more...



### **ENERGY CONVERSION AND STORAGE**

Focusing on all aspects of static and dynamic energy conversion, energy storage, photovoltaics, solar fuels, batteries, capacitors, thermoelectrics, and more...

# Ultrafast terahertz transmission ellipsometry of $\text{YMn}_2\text{O}_5$ electromagnons

Hyosub Kim,<sup>1</sup> Minwoo Yi,<sup>1</sup> Xueyun Wang,<sup>2</sup> Sang-Wook Cheong,<sup>2</sup> and Jaewook Ahn<sup>1,a)</sup>

<sup>1</sup>Department of Physics, KAIST, Daejeon 305-701, South Korea

<sup>2</sup>Rutgers Center for Emergent Materials and Department of Physics and Astronomy, Rutgers University, Piscataway, New Jersey 08854, USA

(Received 4 November 2012; accepted 30 November 2012; published online 13 December 2012)

Terahertz time-domain polarization measurement experiments probe the electromagnon excitations in an orthorhombic multiferroic  $\text{YMn}_2\text{O}_5$ . Spectral phase rotation function measured from the mutually orthogonal polarization components of transmitted probe pulses sensitively resolves the electromagnon resonances which appear unresolvable in conventional transmission spectroscopy. The retrieved oscillator parameters based on electro-optic effects in a lossy birefringent material show good agreement with the previously reported Fourier transform infrared spectroscopy data.

© 2012 American Institute of Physics. [<http://dx.doi.org/10.1063/1.4772206>]

Terahertz time-domain spectroscopy (THz-TDS) has been widely adopted as a linear polarization spectroscopic tool because of its robust, compact, and sensitive spectroscopic capability compared to other far-infrared means.<sup>1-4</sup> The broad spectral range of THz-TDS is efficient to extract oscillator parameters, especially, when being coupled with FT-IR measurements.<sup>5,6</sup> Also, its time-domain and field detection scheme makes it available to extend the realm of research to time-domain polarization study. Researchers have considered polarization-dependent THz-TDS for investigations of ultrafast polarization states,<sup>7,8</sup> material birefringency,<sup>9</sup> polarization sensitive imaging,<sup>10</sup> Kerr effect in topological insulators,<sup>11</sup> Faraday rotation in cuprate superconductors,<sup>12</sup> as well as conventional transmission ellipsometry.<sup>13</sup>

In this letter, we present a oscillator parameter extraction method, based on polarization-specific spectral phase measurements in a THz-TDS setup with a pair of cross polarizers, as shown in Fig. 1. This method, in particular useful for strongly absorptive birefringent materials, takes advantage of the fact that the phase of  $\tilde{E}_y(\omega)/\tilde{E}_x(\omega)$ , where  $\tilde{E}_{x,y}(\omega)$  are the spectral amplitudes of the *x*- and *y*-polarization components of a transmitted THz pulse, rapidly shifts near an absorption frequency. In experiments carried out with an orthorhombic multiferroic  $\text{YMn}_2\text{O}_5$  single crystal, two resonant absorption peaks at 490 and 590 GHz are observed, which is in qualitative agreement with the electromagnon modes in the incommensurate magnetic and ferroelectric phase of this material at temperature below 20 K.<sup>14</sup>

We consider a linearly polarized THz pulse is normally incident on a target medium with a slightly tilted polarization angle of  $\theta$  from the slow axis, which is crucial in this experiment. The spectral amplitude of the THz pulse after through the medium is then given by

$$\tilde{E}(\omega)(\hat{n}_2\tilde{t}_2e^{i\hat{n}_2\omega d/c}\cos\theta - \hat{n}_1\tilde{t}_1e^{i\hat{n}_1\omega d/c}\sin\theta), \quad (1)$$

where  $d$  is the thickness of the medium,  $c$  is the speed of light,  $\tilde{t}_{1,2} = 4\hat{n}_{1,2}/(1 + \hat{n}_{1,2})^2$  are the Fresnel coefficient for transmission,  $\hat{n}_{1,2}$  and  $\tilde{n}_{1,2}$  are the directions and the refractive

indexes of the fast and slow axes, respectively. After the THz pulse is projected on to two polarization directions  $\hat{x}$  and  $\hat{y}$ , respectively, by an analyzing polarizer, where for simplicity the angle between  $\hat{x}$  ( $\hat{y}$ ) and  $\hat{n}_2$  is chosen as  $\pi/4$  ( $-\pi/4$ ), we measure the polarization components  $\tilde{E}_x(\omega)$  and  $\tilde{E}_y(\omega)$  to obtain their phase difference  $\Delta\phi(\omega) = \tan^{-1}(\tilde{E}_y/\tilde{E}_x)$ , where

$$\frac{\tilde{E}_y(\omega)}{\tilde{E}_x(\omega)} = \frac{1 + \frac{\tilde{t}_1}{\tilde{t}_2}e^{i\Delta\tilde{n}\omega d/c}\tan\theta}{1 - \frac{\tilde{t}_1}{\tilde{t}_2}e^{i\Delta\tilde{n}\omega d/c}\tan\theta} \quad (2)$$

with  $\Delta\tilde{n} = \tilde{n}_1 - \tilde{n}_2$ . When the birefringent medium is lossless,  $\Delta\phi(\omega)$  remains near zero for any frequency but, when a large spectral absorption in  $\hat{n}_{2(1)}$  is introduced, on the other hand, the phase of  $\tilde{E}_y(\omega)/\tilde{E}_x(\omega)$  starts to rapidly shift near the absorption frequency.

In a  $\text{YMn}_2\text{O}_5$  crystal, there exist three magnetic phases: an incommensurate magnetic and ferroelectric phase (LT1) below 20 K; a commensurate magnetic and ferroelectric phase (LT2) from 20 to 40 K; and a paramagnetic-paraelectric phase above 45 K (LT3).<sup>15,16</sup> It has been reported that in the lowest

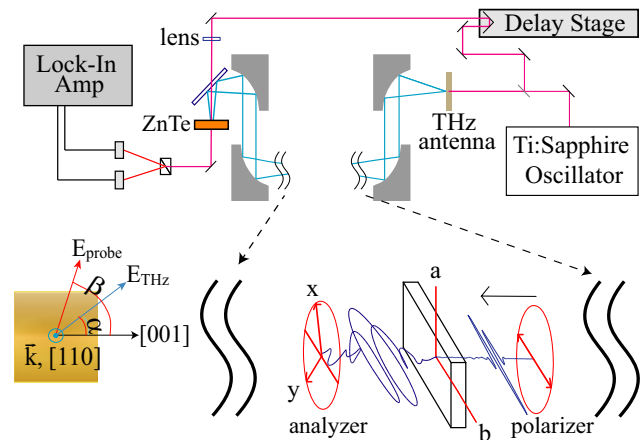


FIG. 1. Ultrafast THz transmission ellipsometry configuration. The analyzer polarization is set to  $\pm\pi/4$  for acquiring the complete three-dimensional profile of THz pulses. Inset shows the polarization angles of the optical probe and THz pulses.

<sup>a)</sup>Electronic mail: jwahn@kaist.ac.kr.

temperature phase of LT1, there are three resonant absorption peaks in THz frequency range, so called electro-magnons at 216, 500, and 610 GHz, respectively, which are electric-dipole active only along the  $b$  (slow) crystal axis.<sup>14</sup> Thus, the permeability is  $\mu_b = 1$  and the permittivity  $\epsilon_b(\omega)$  is given as a sum of Lorentz oscillators, *i.e.*,

$$\epsilon_b(\omega) = \epsilon_b(\infty) + \sum_j \frac{S_j}{\omega_j^2 - \omega^2 - i\omega\gamma_j}, \quad (3)$$

where  $\epsilon_b(\infty)$  is the high frequency permittivity,  $S_j$ ,  $\omega_j$ , and  $\gamma_j$  are the oscillator strength, the resonant frequency, and the line width of  $j$ th oscillator, respectively.

Experiment was performed in a conventional THz-TDS setup with an additional pair of polarizers for polarization analysis, as shown in Fig. 1. The laser source was an ultrafast laser oscillator operating at a pulse repetition rate of 80 MHz to produce 100-fs-short pulses. The laser spectrum was centered at a wavelength of 850 nm. The generation and detection of THz pulses were carried out by a photo-conductive antenna (PCA) and a ZnTe electro-optic sampler, respectively. When the PCA being biased by square electrical pulses modulated at a frequency of 65 kHz was illuminated by ultrafast optical pulses, linearly polarized THz pulses with a broad spectrum in 0.1–1.5 THz were produced. The emitted THz pulses were then guided by four off-axis parabolic mirrors and spectroscopy was performed at the configuration focus. The sample was mounted on the liquid helium cooled finger-type transmission cryostat. Before and after the cryostat, a pair of wire-grid terahertz polarizers of 10  $\mu\text{m}$  wire thickness and 25  $\mu\text{m}$  spacing were installed. The first polarizer set incident THz polarization and the second was used to record the polarization information of the propagating THz pulses. The THz pulses were then focused on to the [110]-cut 2-mm-thick ZnTe crystal simultaneously overlapped with an optical probe beam. After the probe beam was split into two by a Wollaston prism, a balanced lock-in amplification detection was performed seeded by the THz modulation frequency. The whole setup was covered by an acryl box and purged with dry air to eliminate water vapor absorptions. In an electro-optic sampling for THz electric field measurement by a ZnTe crystal, the electric field amplitude is given by

$$E_{\text{THz}} \propto \cos \alpha \sin 2\beta + 2 \sin \alpha \cos 2\beta, \quad (4)$$

where  $\alpha$  and  $\beta$  are angles for the polarization directions, respectively, of the THz pulse and the probe optical pulse with respect to the [001]-direction of the ZnTe crystal.<sup>17</sup> When the detected signal is maximized in a configuration of  $\alpha = \beta$ , the orthogonal polarization component of the THz pulse is insensitive to the measurement in the given polarization scheme.<sup>9</sup>

Once the crystallographic  $b$ -axis of the crystal was slightly tilted from the incident THz polarization by an angle  $\theta \approx 6^\circ$ , with the two orthogonal analyzing axes,  $\hat{x}$  and  $\hat{y}$ , respectively,  $\tilde{E}_y(\omega)$  and  $\tilde{E}_x(\omega)$  were measured to reconstruct the complete time-domain polarization information of the transmitted pulse. A typical three-dimensional profile of a THz pulse is shown in Fig. 2(a). The transmission was then

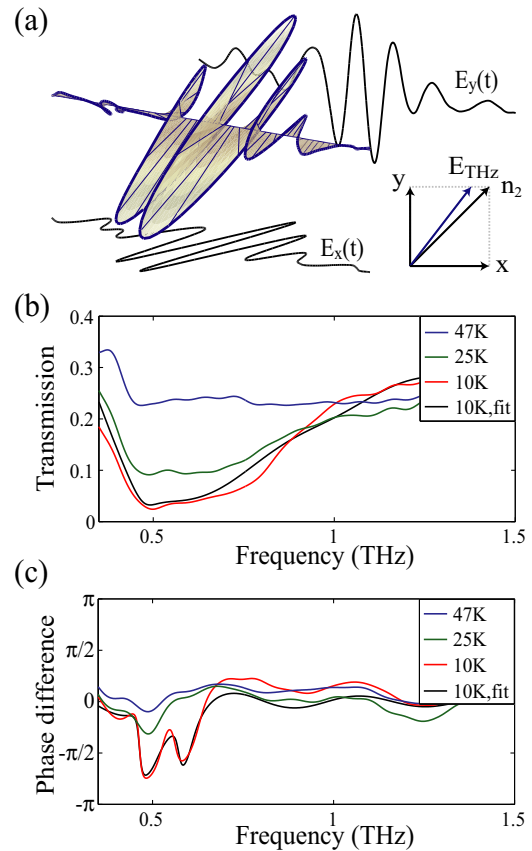


FIG. 2. (a) Time-domain profile of transmitted THz pulses through the  $\text{YMn}_2\text{O}_5$  crystal with the  $b$  axis tilted by  $\theta = \pi/30$  from the incident linear polarization direction. (b and c) Experimental data of  $\text{YMn}_2\text{O}_5$  in three material phases. Transmission spectrum is acquired whence the analyzer angle is set to 0. A broad electromagnon absorption in the LT1 phase is clearly deviated into two peaks in phase difference measurement.

measured by setting the angle of the analyzer at  $0^\circ$  and also the phase difference  $\Delta\phi(\omega)$  were calculated from the angle of  $\tilde{E}_y(\omega)/\tilde{E}_x(\omega)$ . Figure 2(b) shows the measured transmission spectra for the three material phases, LT1, LT2, and LT3, along with the oscillator fitting curve for the LT1 spectrum. The lower frequency region below 0.35 THz is not reliable because of the diffraction loss due to the small size of the sample. Within the measurable spectral range, only two oscillators within a given frequency window are considered here, and the lowest frequency electromagnon at 216 GHz and the phononic absorption at 3.4 THz are not.<sup>14</sup> Thus a broad background absorption from phononic tails is compensated by inserting a constant imaginary  $\epsilon_2$  otherwise it introduces critical mismatch in transmission spectrum. Fig. 2(c) presents the spectral phase difference for the three material phases, respectively, along with the oscillator fitting of the LT1 case. The phase difference  $\Delta\phi(\omega)$  measurement shows the sharp feature of the two absorption peaks, while the transmission in Fig. 2(b) shows broad and blurred absorption behavior.

Numerical extraction of the oscillator parameters from the measured  $\Delta\phi(\omega)$  was performed as following: Starting with the initial oscillator parameters extracted from the transmission data, we calculated  $\Delta\phi'(\omega)$ . Then, the difference between  $\Delta\phi'(\omega)$  and  $\Delta\phi(\omega)$  was minimized adaptively by adjusting the oscillator parameters until minimal deviation

TABLE I. Oscillator parameters.

Case	$\omega_{1,2}$ (THz)	$S_{1,2}$ (THz <sup>-2</sup> )	$\gamma_{1,2}$ (THz <sup>-1</sup> )
Transmission	0.48	0.022	0.091
	0.58	0.34	0.50
Phase	0.49	0.082	0.11
	0.59	0.043	0.076

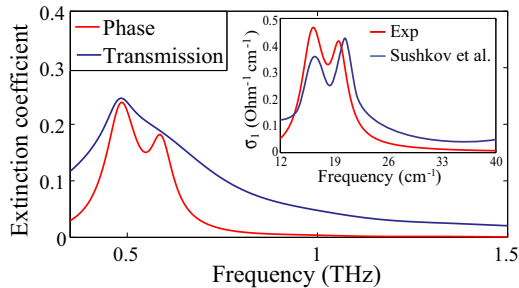


FIG. 3. Extinction coefficient curves of  $\text{YMn}_2\text{O}_5$ , respectively, acquired from the transmission and phase information measured at 10 K. Inset shows comparison between the present results and Sushkov *et al.*'s.<sup>14</sup>

was reached. The large deviation at off-resonance frequency range comes obviously from the high-frequency phonon absorptions unmeasured due to the limited spectral range. The inset shows the comparison between the previously reported measurement<sup>14</sup> and the present phase measurement-based fitting. The obtained oscillator parameters, respectively, from the transmission and phase measurements, are listed in Table I, and the resulting extinction coefficients are plotted in Fig. 3. The direct comparison clearly shows a dramatically increased resolution in the phase measurement case.

Although unmeasurable high frequency phonon information and the diffraction loss introduce a fundamental inaccuracy of our oscillator parameter extraction, the comparable magnitude and spectral resolution shows the phase measurement-based oscillator parameter extraction method works with reliability. In the present experiment, the blurred peaks in transmission data comes mainly from the sample thickness (1.2 mm), and thus the severe decrease of signal to noise ratio near the absorptive range. However, in the case of phase difference measurement, the comparison between two polarization signals gives a kind of balancing, so an improved resolving power is achieved. One drawback of the presented method might be the requirement of a *a priori* infor-

mation of the refractive index of the other axis (fast) and the complex fitting equation. However, as demonstrated, the dramatical improvement in resolution of two adjacent resonant peaks makes this method worthwhile.

In conclusion, we presented an oscillator parameter fitting method utilizing the phase measurement in an ultrafast THz transmission ellipsometry setup, and showed such a transmission ellipsometry-type method could improve correctness of the oscillator parameters compared with the mere transmission measurement in the case of absorptive birefringent samples.

This research was supported in part by Basic Science Research Programs [2010-0013899 and 2009-0083512] and in part by the WCI Program [WCI 2011-001] through the National Research Foundation of Korea. Work at Rutgers was supported by DOE under Contract No. DE-FG02-07ER46382.

- <sup>1</sup>D. Grischkowsky, S. Keiding, M. van Exter, and C. Fattinger, *J. Opt. Soc. Am. B* **10**, 2006 (1990).
- <sup>2</sup>D. M. Mittleman, R. H. Jacobsen, R. Neelamani, R. G. Baraniuk, and M. C. Nuss, *Appl. Phys. B* **67**, 379–390 (1998).
- <sup>3</sup>T. Jeon, K. Kim, C. Kang, S. Oh, J. Son, K. An, D. Bae, and Y. Lee, *Appl. Phys. Lett.* **80**, 3403 (2002).
- <sup>4</sup>M. Naftaly and R. E. Miles, *Proc. IEEE* **95**, 1658 (2007).
- <sup>5</sup>Y. Chen, H. Liu, Y. Deng, D. Schauki, M. J. Fitch, R. Osiander, C. Dodson, J. B. Spicer, M. Shur, and X.-C. Zhang, *Chem. Phys. Lett.* **400**, 357 (2004).
- <sup>6</sup>F. Huang, B. Schulkin, H. Altan, J. F. Federici, D. Gary, R. Barat, D. Zimdars, M. Chen, and D. B. Tanner, *Appl. Phys. Lett.* **85**, 5535 (2004).
- <sup>7</sup>K. Lee, M. Yi, J. D. Song, and J. Ahn, *Opt. Express* **20**, 12463 (2012).
- <sup>8</sup>X. Lu and X.-C. Zhang, *Phys. Rev. Lett.* **108**, 123903 (2012).
- <sup>9</sup>L. Zhang, H. Zhong, C. Deng, C. Zhang, and Y. Zhao, *Appl. Phys. Lett.* **94**, 211106 (2009).
- <sup>10</sup>S. Katletz, M. Pfefer, H. Pühringer, M. Mikulics, N. Vieweg, O. Peters, B. Scherger, M. Scheller, M. Koch, and K. Wiesauer, *Opt. Express* **20**, 23025 (2012).
- <sup>11</sup>R. V. Aguilar, A. V. Stier, W. Liu, L. S. Bilbro, D. K. George, N. Bansal, L. Wu, J. Cerne, A. G. Markelz, S. Oh, and N. P. Armitage, *Phys. Rev. Lett.* **108**, 087403 (2012).
- <sup>12</sup>S. Spielman, B. Parks, J. Orenstein, D. T. Nemeth, F. Ludwig, J. Clarke, P. Merchant, and D. J. Lew, *Phys. Rev. Lett.* **73**, 1537 (1994).
- <sup>13</sup>M. J. Paul, N. A. Kuhta, J. L. Tomaino, A. D. Jameson, L. P. Maizy, T. Sharf, N. L. Rupasinghe, K. B. K. Teo, S. Inampudi, V. A. Podolskiy, E. D. Minot, and Y.-S. Lee, *Appl. Phys. Lett.* **101**, 111107 (2012).
- <sup>14</sup>A. B. Sushkov, R. V. Aguilar, S. Park, S.-W. Cheong, and H. D. Drew, *Phys. Rev. Lett.* **98**, 027202 (2007).
- <sup>15</sup>N. Hur, S. Park, P. A. Sharma, J. S. Ahn, S. Guha, and S.-W. Cheong, *Nature* **429**, 392 (2004).
- <sup>16</sup>L. C. Chapon, P. G. Radaelli, G. R. Blake, S. Park, and S.-W. Cheong, *Phys. Rev. Lett.* **96**, 097601 (2006).
- <sup>17</sup>P. C. M. Planken, H. Nienhuys, H. J. Bakker, and T. Wennebach, *J. Opt. Soc. Am. B* **18**, 313 (2001).